Astrophysical *S* factor for α capture on ^{117}Sn

I. Căta-Danil,[1] D. Filipescu,[1] M. Ivaşcu,[1] D. Bucurescu,[1] N. V. Zamfir,[1] T. Glodariu,[1] L. Stroe,[1]
G. Căta-Danil,[1,2] D. G. Ghiţă,[1] C. Mihai,[1] G. Suliman,[1] and T. Sava[1]

[1]*Horia-Hulubei National Institute for Physics and Nuclear Engineering, Măgurele-Ilfov, România*
[2]*Physics Department, University Politehnica of Bucharest, România*

The cross sections of the ^{117}Sn$(\alpha, \gamma)^{121}$Te and ^{117}Sn$(\alpha, p)^{120}$Sb reactions have been measured in the effective center of mass energy from 11.5 to 14.6 MeV. Highly enriched self-supporting ^{117}Sn (90%) foils were bombarded with an α beam delivered by the Bucharest IFIN-HH tandem accelerator. The induced activity of ^{121}Te and ^{120}Sb was measured with two large-volume high-purity Ge detectors in close geometry to maximize the detector efficiency. The experimental cross section and astrophysical *S* factor are compared with statistical model predictions for different global α-nucleus optical potentials.

I. INTRODUCTION

The proton-rich nuclei heavier than Fe (the so-called *p*- nuclei) are produced by a combination of the (γ, n), (γ, p) and (γ, α) reactions on existing *s* or *r* nuclei at temperatures around a few GK, characteristic of explosive environments. To adequately describe the *p*-process nucleosynthesis, one needs reliable information on the thousands of reaction rates involved. In this respect, there is a considerable lack of experimental data on the relevant cross sections in the *p*-process energy range, because most γ-induced reactions are very difficult to measure directly [1]. To overcome this difficulty, the charged particle induced reaction cross sections are measured and their inverse photodisintegration reaction cross sections are calculated using the detailed balance theorem [2]. Experimental data for charged particle induced reaction cross sections are scarce above Fe. This is because for nuclei with $Z > 28$ the energies of α-capture reactions are well below the Coulomb barrier, making the cross section very small and thus difficult to measure. However, some measurements were performed and the results of α-capture on ^{63}Cu, ^{70}Ge, ^{96}Ru, ^{106}Cd, ^{112}Sn, and ^{118}Sn can be found in Refs. [3–9].

p-process studies are based mostly on the Hauser-Feshbach statistical model to predict the reaction rates. Although the (p, γ) measurements generally agree with the statistical model prediction within a factor of less than 2, (α, γ) measurements show considerable underestimation compared to a frequently used model prediction [10]. Therefore, it is important to investigate the α-induced reaction cross sections experimentally to test the reliability of the statistical model prediction.

The stellar abundances of $^{115-117}$Sn are underestimated by *s*-process calculations [11]. In the case of ^{115}Sn, it is estimated that the *s*- and *r*-processes can account for only 50% of the abundance [12], and recent *p*-process calculations cannot explain the remaining fraction [13,14]. ^{116}Sn, one of the few so-called *s*-only isotopes (nuclides produced solely by the *s*-process) is a possible calibration point for *s*-process models. However, the *s*-process calculations slightly underestimate the stellar abundance of ^{116}Sn, the difference being explained by a small contribution from the *p*-process

[15]. In this respect, the measurement of the (α, γ) cross sections on proton-rich Sn isotopes gives insight into the (γ, α) cross sections and implicitly into the dilemma involving the *p*-process contribution to the formation of these nuclei. Because the level density decreases at closed shells, these reactions and those involving tin isotopes are also good test candidates for the statistical model assumptions at energies implied by stellar processes. Furthermore, extended experimental cross section data on tin isotopes give a higher reliability in deriving global optical model parametrizations.

The reason for the work presented here is to extend the experimental database by measuring with high precision the (α, γ) capture cross section on the ^{117}Sn isotope in the energy range from 11 to 15 MeV, close to the Gamow peak energy of 8.6 MeV.

In our work, the cross section measurements and the deduced *S* factors are compared with results obtained using the SCAT optical model code [16] combined with the GNASH-FKK statistical model code [17], and with the results of the NONSMOKER statistical model code [18] calculated with standard input parameters.

The details of the experimental procedure and the experimental results are presented and discussed as follows.

II. MEASUREMENTS

A. Experimental method

The characteristic activity from the reaction ^{117}Sn$(\alpha, \gamma)^{121}$Te was measured with a pair of large-volume Ge detectors in close geometry to maximize the detector efficiency. In this case the activation technique involves the bombarding of a target with α particles to produce radioactive species and the measurement of their specific activities after the irradiation has stopped. The details of the activation method and data analysis can be found in our previous papers [19,20].

During irradiation time, ^{121}Te nuclei are obtained in both ground $(1/2^+, 19.16$ d$)$ and isomeric $(11/2^-, 154$ d$)$ states via α capture. The number of nuclei populated on isomeric, N_M, and ground state, N_G, during irradiation has the following

dependence:

$$\frac{dN_M}{dt} = \sigma_M \Phi(t) N_T - \lambda_M N_M(t), \tag{1}$$

$$\frac{dN_G}{dt} = \sigma_G \Phi(t) N_T + f_\gamma \lambda_M N_M(t) - \lambda_G N_G(t), \tag{2}$$

where σ_M and σ_G are the partial capture cross sections to the isomeric and ground states, λ_M and λ_G are the corresponding decay constants, $\Phi(t)$ denotes the α beam flux at the irradiation time t, and f_γ is the decay branch from the isomeric to the ground state (89%) [21]. In these relations, we made the assumption that the number of target nuclei N_T does not vary significantly during irradiation time, which is valid if the condition $\sigma \Phi \ll 1$ is satisfied.

If previous equations are integrated, we obtain the following expressions for the total number of nuclei populated on the isomeric and ground states at the end of the irradiation time t_a:

$$N_M(t_a) = \sigma_M N_T e^{-\lambda_M t_a} \int_0^{t_a} e^{\lambda_M t} \Phi(t)\, dt, \tag{3}$$

$$N_G(t_a) = \sigma_G N_T e^{-\lambda_G t_a} \int_0^{t_a} e^{\lambda_G t} \Phi(t)\, dt + f_\gamma \lambda_M \sigma_M N_T e^{-\lambda_G t_a}$$

$$\times \int_0^{t_a} e^{(\lambda_G - \lambda_M)t} \int_0^{t} e^{\lambda_M t'} \Phi(t')\, dt'. \tag{4}$$

It is obvious that in these relations, the terms $N_T \Phi(t)$ can be replaced with

$$N_T \Phi(t) = p\, \frac{\rho\, h\, N_A}{Z_P\, A_T\, e} I(t), \tag{5}$$

where p is the isotopic enrichment of the ^{117}Sn target (90%); ρh the target's specific thickness; N_A, the Avogadro number; Z_P, the projectile atomic number; A_T, the target mass number; e, the electron charge; and $I(t)$, the electrical beam intensity.

If the target is measured after a waiting time t_w, during the measuring time t_m, the following numbers of ^{121}Te nuclei will be disintegrated from the isomeric and ground states, respectively:

$$N_M^{\text{dez}}(t_w, t_m)$$
$$= N_M^i e^{-\lambda_M t_w}(1 - e^{-\lambda_M t_m}), \tag{6}$$

$$N_G^{\text{dez}}(t_w, t_m)$$

$$= N_G^i e^{-\lambda_G t_w}(1 - e^{-\lambda_G t_m}) + \frac{f_\gamma \lambda_M \lambda_G N_M^i}{\lambda_M - \lambda_G}$$

$$\times \left[\frac{e^{-\lambda_G t_w}(1 - e^{-\lambda_G t_m})}{\lambda_G} - \frac{e^{-\lambda_M t_w}(1 - e^{-\lambda_M t_m})}{\lambda_M} \right], \tag{7}$$

with N_M^i and N_G^i obtained from Eqs. (3) and (4).

These numbers can be connected directly with the peak surface A_i of a certain γ radiation γ_i, which has to be emitted only in the case of isomeric state decay if we are referring to N_M^{dez}, or of the ground state decay in the case of N_G^{dez}, that is,

$$A_i = I_{\gamma_i} \varepsilon_i N_{M,G}^{\text{dez}}(t_w, t_m), \tag{8}$$

where ε_i represents absolute peak efficiency for γ_i radiation in the specified detection geometry, and I_{γ_i} is the absolute γ-ray intensity of γ_i radiation.

TABLE I. Nuclear data used to obtain experimental (α, γ) and (α, p) cross sections [21].

Nuclear reaction	$T_{1/2}$ (days)	E_γ (keV)	I_γ (%)
^{117}Sn$(\alpha, \gamma)^{121}$Te^m	154 (7)	212.189	81.4 (11)
^{117}Sn$(\alpha, \gamma)^{121}$Te$^{\text{g.s.}}$	19.16 (5)	507.591,	17.8 (9),
		573.139	80.30 (25)
^{117}Sn$(\alpha, p)^{120}$Sb^m	5.76 (2)	89.8,	79.5 (16),
		197.3,	87.0 (11),
		1023.3	99.4 (3)
^{48}Ti$(\alpha, n)^{51}$Cr	27.7010 (11)	320.10	9.91 (1)

When the ^{117}Sn isotope is irradiated with α particles, in the studied energy range, besides the (α, γ) capture reaction, the ^{117}Sn$(\alpha, n)^{120}$Te and ^{117}Sn$(\alpha, p)^{120}$Sb reactions are also taking place. For the (α, n) reaction, we cannot determine the cross section using this method, because the ^{120}Te isotope created in this way is stable and does not have any isomeric levels. But for the (α, p) reaction, the ^{120}Sb isotope has an isomeric level (8^-) with a half-life of 5.76 d. Both isomeric and ground states decay through β^+ and EC processes. Unfortunately, the ground state has a small half-life in the context of this experiment (15.89 min) and is decaying mainly (98.3%) to the ^{120}Sn ground state with a very small amount of emitted γ rays. Consequently, it was not possible to obtain the cross section for the ^{117}Sn$(\alpha, p)^{120}$Sb$^{\text{g.s.}}$ reaction. In the case of isomeric level decay, there are some γ rays emitted with enough intensity by the β daughter (^{120}Sn), a fact that made it possible to obtain the cross section for the ^{117}Sn$(\alpha, p)^{120}$Sb^m reaction. This goal was achieved using the same procedure mentioned above for the (α, γ) capture reaction on the isomeric level of ^{121}Te.

The main nuclear data needed to obtain the cross sections are given in Table I.

B. Target preparation

Isotopically enriched tin targets having 3.95% ^{116}Sn, 90% ^{117}Sn, 3.81% ^{118}Sn, 1.71% ^{119}Sn, and 0.53% ^{120}Sn in the form of self-supporting foils of $\sim$4.5 mg/cm^2 were used in this experiment. The highly enriched ^{117}Sn targets were prepared via mechanical rolling. The ^{117}Sn foils were mounted on circular Al holders with a hole diameter of 12 mm. A stack was prepared having three ^{117}Sn targets alternating with aluminum foils of thickness $\sim$5.5 mg/cm^2. A titanium foil of 3 mg/cm^2 was placed at the end of the stack. The aluminum foils served as incident α-beam energy degraders and as catchers for recoil nuclei from the ^{117}Sn foils to estimate the recoil fraction. The titanium foil was used to measure the ^{48}Ti$(\alpha, n)^{51}$Cr cross section. The measured cross section was used to verify the beam current integration by comparing our data with that from Ref. [22].

Target thickness has a very important role in this experiment, primarily because it appears directly in relations used to compute the cross section [see Eq. (5)] but also as it defines the energy (and the energy spread) at which the cross sections are measured.

For this purpose, besides weighing the targets, we made an additional α transmission experiment. The α source consisted

TABLE II. Targets thickness and irradiation energies of each foil.

Target No.	Thickness (μm)	Specific thickness (mg/cm^2)	Energy (MeV) First campaign	Second campaign
Sn #1	6.4	4.660	14.5 ± 0.1	
Al #2	21.15	5.715	13.2 ± 0.2	
Sn #3	6.45	4.697	11.9 ± 0.2	
Al #4	21.30	5.755	10.3 ± 0.2	
Sn #5/#1	5.95	4.333	8.8 ± 0.2	15.1 ± 0.1
Ti #6/#2	6.70	3.028	7.8 ± 0.2	14.4 ± 0.1

of a mixture of ^{241}Am and ^{244}Cm. The energy spectra of transmitted α particles through the Sn foils were measured with a totally depleted silicon detector. Target thicknesses were obtained by performing successive TRIM [23] simulations until we managed to reproduce the shifted energy spectrum, considering the direct spectrum as an input for the TRIM code. Target thicknesses obtained in this experiment were consistent with the ones obtained by weighing, and the values are reproduced in Table II.

C. Activations and data analysis

The stack was mounted in a Faraday cup, isolated from the rest of the beamline, and bombarded with a ^{4}He^{2+} beam from the IFIN-HH tandem accelerator. To get an accurate measurement, a ring was placed at the Faraday cup entrance having a -300 V bias voltage designated to suppress secondary electrons.

The energy of the incident α particles covered a range between 8.7 and 15 MeV. These energies are particularly interesting because the Gamow peak of the ^{117}Sn$(\alpha, \gamma)^{121}$Te reaction at $T_9 = 3$ GK is estimated to be at 8.6 MeV with a width of 3.4 MeV. For α-induced reactions on ^{117}Sn, the activation technique is suitable to determine the cross section, because the reaction products are radioactive with convenient half-lives (19.16 d for ^{121}Te$^{g.s.}$, 154 d for ^{121}Te^m, and 5.76 d for ^{120}Sb^m) as given in Table I.

We performed two experiments. In the first experiment, a stack of three ^{117}Sn foils interspaced by two aluminum foils ended with a Ti foil were irradiated with a 15 MeV ^{4}He^{2+} beam. The incident beam energies and straggling on the successive target foils were determined based on the energy loss in the aluminum and ^{117}Sn foils using dE/dx values obtained using the TRIM code. Figure 1 illustrates energy spectra of α particles inside of ^{117}Sn and ^{48}Ti foils simulated with TRIM code. As we can see in this figure, the α beam energy spectrum within the fifth foil is centered on a value of 8.76 MeV. At this energy situated significantly below Coulomb barrier ($\sim$17.8 MeV), we were not able to observe any of the γ lines specified in Table I. We performed a second experiment in which a stack consisting of a ^{117}Sn foil followed by a Ti one was irradiated with a 15.6 MeV ^{4}He^{2+} beam. In Table II, mean values and widths of α energy spectra within all irradiated foils are given, too.
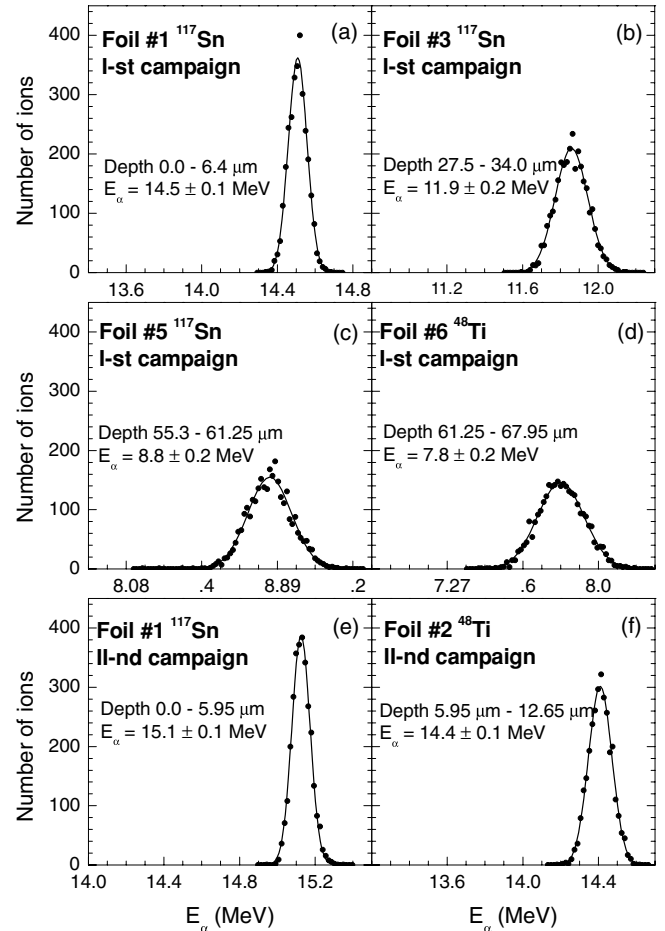
FIG. 1. Energy spectra of α particles inside of ^{117}Sn and ^{48}Ti foils simulated with the TRIM code.

Another important parameter needed to perform the calculations is the beam intensity and its time dependence. The beam current was acquired in real time using an ORTEC 439 digital current integrator in steps of one second, small enough to perform the integration. The typical current was between 20 and 25 nA as can be seen in Fig. 2.

We also determined the ^{48}Ti$(\alpha, n)^{51}$Cr cross section using the 320 keV γ line emitted by ^{51}V, which resulted from EC decay of ^{51}Cr, and for validation purposes we compared our results with experimental data points obtained by Morton [22] at the same energies.

All measurements have been performed with a specially designed low-background setup—both detectors were surrounded with Pb walls clothed with Cu and Al plates on the inside. For the dead-time correction, we used a pulse generator with a fixed frequency of the output signal (20 Hz). Efficiency calibration of HPGe detectors was done using calibrated point sources of ^{152}Eu, ^{133}Ba, ^{241}Am, ^{60}Co, and ^{137}Cs, placed in the same geometry as the targets. We also took into account the summing effects due to the close geometry. This was achieved using the Monte-Carlo simulation code GESPECOR [24]. The calibration curves for both detectors used in the experiment are presented in Fig. 3.
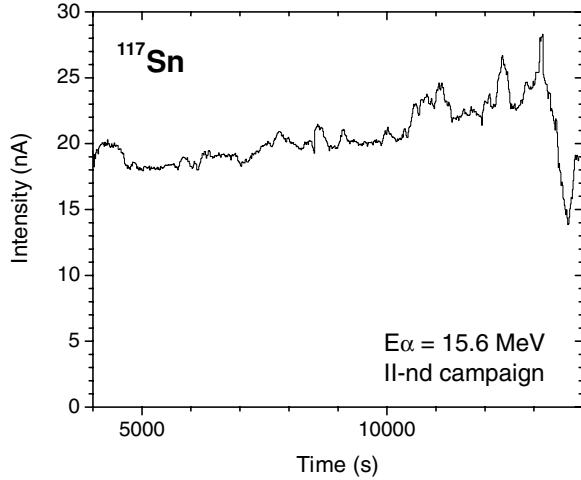
FIG. 2. Time dependence of beam intensity monitored in the second campaign.

Figure 4 presents some partial γ-ray spectra obtained in our experiment including irradiation, waiting, and counting times. Using these spectra, we obtained ^{117}Sn$(\alpha, \gamma)^{121}$Te^m, ^{117}Sn$(\alpha, \gamma)^{121}$Te$^{g.s.}$, and ^{117}Sn$(\alpha, p)^{120}$Sb^m cross sections which are reproduced in Table III.

III. COMPARISON BETWEEN EXPERIMENTAL DATA AND THEORY

A. Optical model calculations

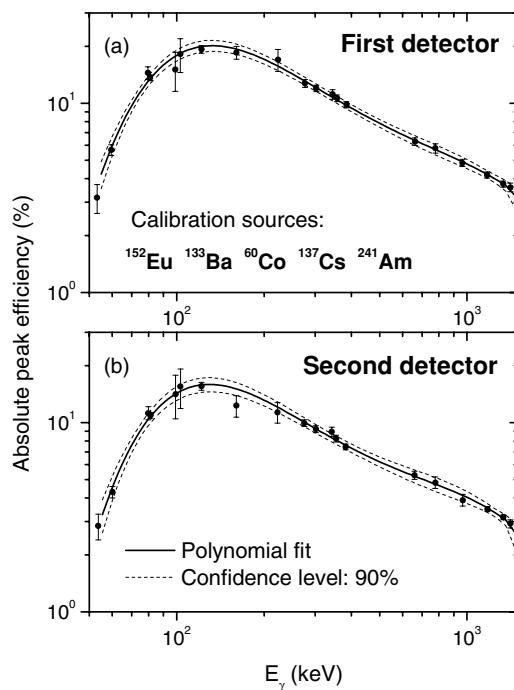Optical model (OM) calculations were done using the SCAT2 code [16]. As already known, the optical model can predict

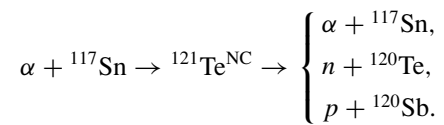FIG. 3. Absolute peak efficiency for both detectors used in our experiment.

TABLE III. Measured cross sections in present experiment.

E_α^{Lab} (MeV)	Cross section (mb)		
	^{117}Sn$(\alpha, \gamma)^{121}$Te^m	^{117}Sn$(\alpha, \gamma)^{121}$Te$^{g.s.}$	^{117}Sn$(\alpha, p)^{120}$Sb^m
15.1 ± 0.1	4.6 ± 0.6	8.3 ± 1.0	0.012 ± 0.002
14.5 ± 0.1	3.2 ± 0.4	6.3 ± 0.8	0.005 ± 0.001
11.9 ± 0.2	0.09 ± 0.01	0.27 ± 0.03	

the following quantities: total cross section, direct elastic cross section, compound cross section, and the transmission coefficients for statistical model calculations. As outlined in Ref. [25], the OM parametrization does not reproduce the α elastic scattering cross section below the Coulomb barrier. We should mention that because the reaction is induced by a charged particle, when we enumerate the above cross sections we refer only to their nuclear part, neglecting the Coulomb part.

In this respect, we used three phenomenological global optical potentials developed for incident α particles: McFadden and Satchler [26], Huizenga [27], and Avrigeanu [25]. Usually, to validate the proper OM parameters for the target and the energy range of the incident particle, a comparison of the experimental data with the total cross section and integrated or differential elastic cross section (at higher energies where the compound elastic contribution to the elastic cross section becomes negligible) provided by the OM is made. In our case, the lack of experimental data made this procedure impossible. However, we tested these potentials on the available experimental data on neighboring isotopes, and we concluded that all three OM potentials give a rather good prediction of the existing experimental data, so we rejected none.

For the statistic model calculation we considered the following channels:

$$\alpha + {}^{117}\mathrm{Sn} \rightarrow {}^{121}\mathrm{Te}^{\mathrm{NC}} \rightarrow \begin{cases} \alpha + {}^{117}\mathrm{Sn}, \\ n + {}^{120}\mathrm{Te}, \\ p + {}^{120}\mathrm{Sb}. \end{cases}$$

Therefore, we need also the transmission coefficients for neutrons and protons from direct reaction on ^{120}Te and ^{120}Sb. For this purpose were used the global optical potential of Köning and Delaroche [28], well known for its accuracy provided for a large range of energy and mass of nuclei. However, because the neutron emission plays a dominant role against all the rest of the opened channels, we tested the accuracy of the neutron transmission coefficients for the $n + {}^{122}$Te reaction for which experimental data exists in the EXFOR database, and we obtained a good agreement of total cross section with experimental data.

B. Statistical model evaluation

The statistical model and preequilibrium calculation were made using the GNASH-FKK code [17].

The first step consisted of selecting the proper number of low-lying discrete levels taken into account for the compound
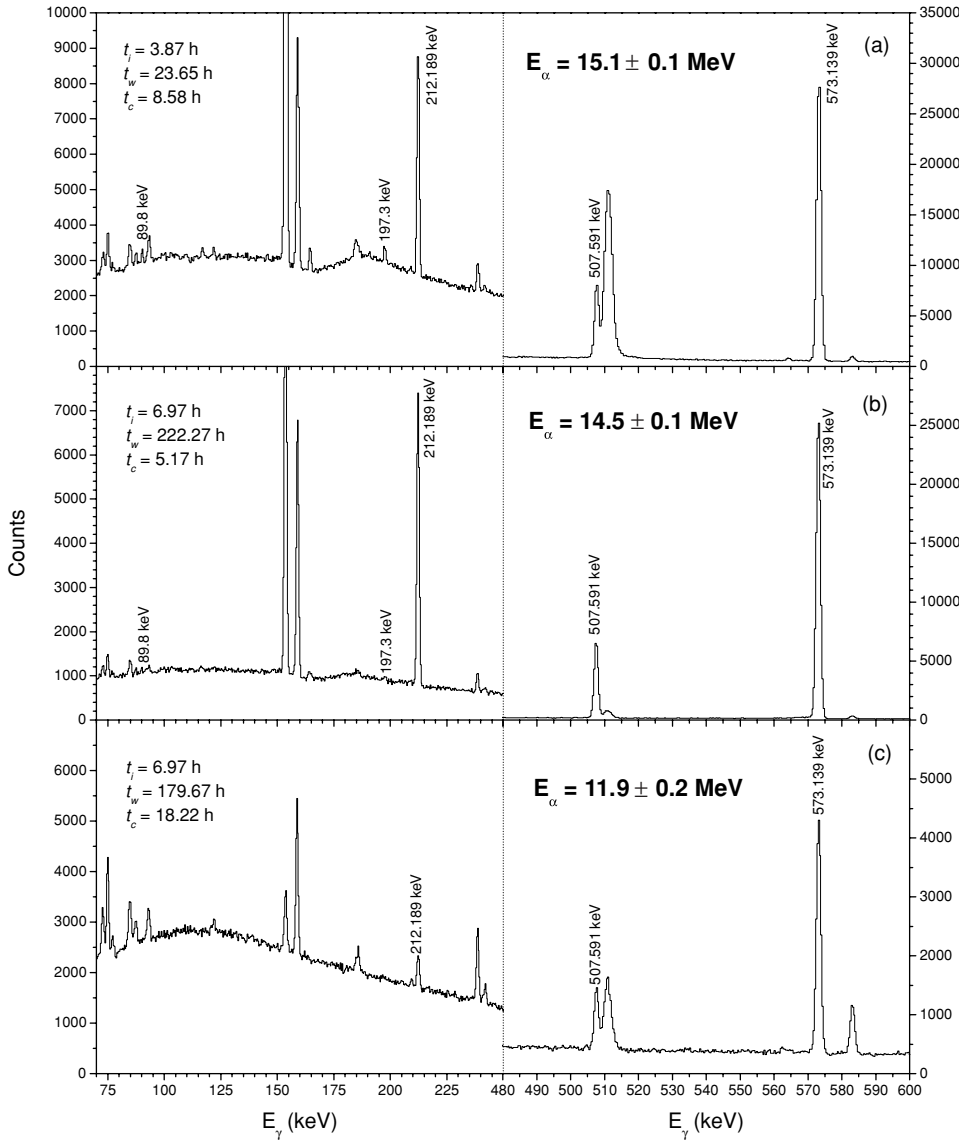
FIG. 4. Some partial HPGe *γ*-ray spectra measured in the present experiment.

nucleus (^{121}Te) and for the three residual nuclei (^{117}Sn, ^{120}Te, and ^{120}Sb). For this purpose we used the RIPL database [29].

This data library contains also levels for which the decay mode is unknown. Usually, to fulfill the sum rule over the cross section (the sum over all calculated cross sections should be equal to the total cross section provided by the OM), it is usual to impose 100% decay of these levels on the ground state. However, in our case, the fact was taken into account that two of the nuclei (^{121}Te and ^{120}Sb) have isomeric states. For this reason, each level with an unknown decay mode was individually analyzed to establish if the most favorable decay is to the ground state or to the isomeric state. This plays a major role in providing an accurate ratio between the cross section population of ground and isomeric states.

Another important ingredient in the estimation of the compound cross sections are the level density parameters. In this case the Gilbert and Cameron formula [30] was used. Usually the level density parameter *a* is obtained through a fitting procedure of the experimental neutron *s*-wave resonance spacing D_0. In the case of residual nuclei, due to the lack of D_0 experimental data, the Gilbert-Cameron systematic was used for the level density parameter *a*. The rest of the level density parameters were derived by imposing that the calculated cumulative number of levels should reproduce the experimental low-lying levels. The related level density parameters are summarized in Table IV.

For estimating the *γ* transmission coefficients, the Kopecky-Uhl giant resonance parametrization [31] of the *γ*-ray strength function was used.

TABLE IV. Level density parameters used in statistical model calculations.

Nucleus	*a* (MeV^{-1})	*T* (MeV)	E_r (MeV)	E_0 (MeV)	No. of discrete levels
^{121}Te	18.358	0.610	5.968	−0.924	37
^{120}Te	18.0	0.590	6.604	0.561	6
^{120}Sb	16.0	0.600	3.744	−1.287	36
^{117}Sn	16.893	0.542	4.316	0.202	23

Due to the lack of experimental information regarding the neutron *s*-wave resonance spacing D_0 and average radiative capture width $\langle \Gamma_s \rangle$ due to the *s*-wave neutron interaction, we used in the first run the default values of the GNASH-FKK code, which correspond to the interpolation table of Kopecky. The calculated radiative capture cross sections underestimate our experimental data for the $^{117}Sn(\alpha, \gamma)^{121}Te^m$ and $^{117}Sn(\alpha, \gamma)^{121}Te^{g.s.}$ reactions. Subsequently, we adjusted the value for the normalization constant $2\pi \langle \Gamma_s \rangle / \langle D_{0s} \rangle$ to provide an accurate description of the $^{117}Sn(\alpha, \gamma)^{121}Te^{g.s.}$ experimental cross section with the calculation, using the McFadden potential. The fact that the adjustment of the normalization constant $2\pi \langle \Gamma_s \rangle / \langle D_{0s} \rangle$ reproduced simultaneously also the $^{117}Sn(\alpha, \gamma)^{121}Te^m$ and $^{117}Sn(\alpha, p)^{120}Sb^m$ validates the level density parameters and at the same time the size of the adjustment. This does not mean necessarily that this potential could provide more accurate results than other ones.

C. Discussion

In Fig. 5 we compare the experimental cross section for the $^{117}Sn(\alpha, \gamma)^{121}Te^m$ and $^{117}Sn(\alpha, \gamma)^{121}Te^{g.s.}$, and $^{117}Sn(\alpha, p)^{120}Sb^m$ reactions with the calculated ones provided by the McFadden potential using the above-mentioned adjustment of the normalization constant $2\pi \langle \Gamma_s \rangle / \langle D_{0s} \rangle$. The figure shows a general agreement within error bars between the calculated and experimental data. It is worth mentioning that the lowest experimental energy point is overestimated by a factor of ~4.

FIG. 6. Comparison between experimental data points and evaluations performed with GNASH (McFadden potential) and NONSMOKER codes.

The good agreement at high energies validates the level density parameters used; therefore the disagreement at low energies can be attributed to the transmission coefficients, thus highlighting the limitations of OM parametrizations below the Coulomb barrier.

Moreover, in Fig. 6 we plot also the calculated values with the NONSMOKER code [18], which is usually used in astrophysical studies. One major inconvenience of these tabulated NONSMOKER values is that we had no information
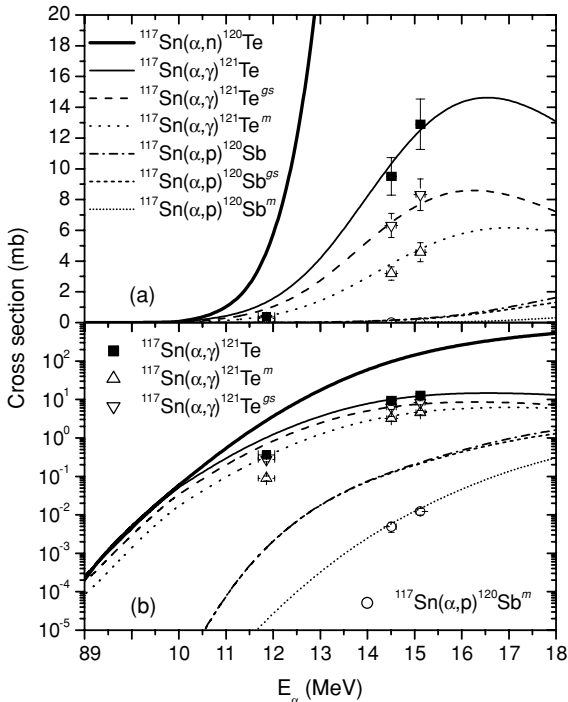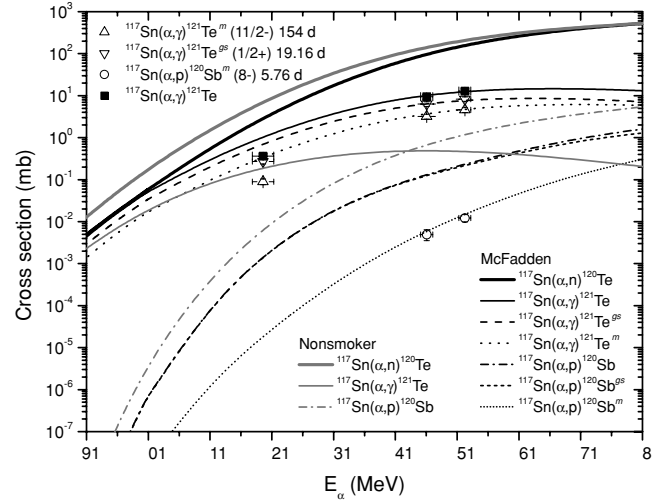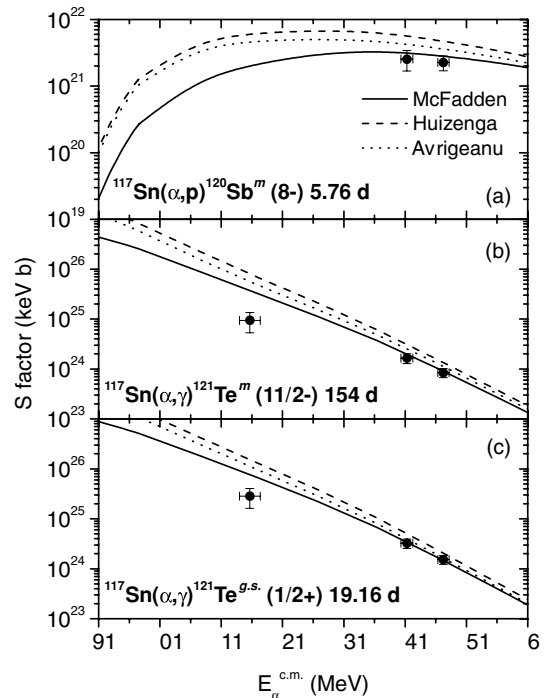

FIG. 5. Cross sections evaluated with the McFadden optical model potential compared with experimental points in linear and logarithmic scales.

FIG. 7. Experimental astrophysical *S* factors for studied reactions compared with theoretical evaluations.

TABLE V. Experimental S factor values for all studied reactions.

$E_{\text{eff}}^{\text{c.m.}}$ (MeV)	S factor ($\times 10^{21}$ keV·b)		
	^{117}Sn$(\alpha, \gamma)^{121}$Te^m	^{117}Sn$(\alpha, \gamma)^{121}$Te$^{\text{g.s.}}$	^{117}Sn$(\alpha, p)^{120}$Sb^m
14.63 ± 0.09	844 ± 173	1533 ± 304	2.3 ± 0.6
14.03 ± 0.10	1645 ± 360	3259 ± 689	2.6 ± 0.9
11.5 ± 0.2	9333 ± 4049	28349 ± 12079	

about the parameters used in the calculation. Another one is, for this particular case, that the tabulated NONSMOKER values report only a total cross section for ^{117}Sn$(\alpha, \gamma)^{121}$Te and ^{117}Sn$(\alpha, p)^{120}$Sb and no information about the population of ground and isomeric states. Nevertheless, the calculated NONSMOKER (α, γ) cross section underestimates both the experimental values and the GNASH-FKK calculation.

It is difficult to trust a certain evaluation as long as there is only our set of experimental values and no others for validation. Furthermore, no trustworthy experimental data of different parameters needed for a reliable evaluation exist. However, if we refer only to the higher energy points, the fact that the evaluation reproduces simultaneously the ^{117}Sn$(\alpha, \gamma)^{121}$Te and ^{117}Sn$(\alpha, p)^{120}$Sb gives credibility to the choice of level density parameters and accordingly to the normalization constant $2\pi \langle \Gamma_s \rangle / \langle D_{0s} \rangle$. An improper choice of these parameters would increase one cross section and decrease the other one, hence making impossible the agreement with both experimental points. With this choice of parameters, the disagreement in the cross section of the ^{117}Sn$(\alpha, \gamma)^{121}$Te at 11.85 MeV can only be attributed to the transmission coefficients calculated with the OM. These limitations of the OM parameters below the Coulomb barrier are typical for the global OM parametrizations available, as outlined in Ref. [25].

We obtained an evaluation of cross sections, based on credible model parameters, that describe our experimental points measured for both the (α, γ) process and the (α, p) process, giving consistency and reliability to the parameter set used in the evaluation process. However, future experiments providing information about the cross section of all open processes in this energy range are needed for a reliable evaluation. In addition, experimental information regarding physical quantities such as neutron s-wave resonance spacing and their average radiative capture width would be essential for establishing a trustworthy validation of the set of parameters used in this mass region.

Finally, from these experimental cross sections we derived the related astrophysical S factors for the three studied reactions. They are presented in Table V and are compared in Fig. 7 with theoretical calculations with SCAT2 and GANSH-FKK using all three sets of OM parameters for the α particle mentioned before.

[1] H. Utsunomiya, P. Mohr, A. Zilges, and M. Rayet, Nucl. Phys. **A777**, 459 (2006).

[2] C. Angulo, M. Arnould, M. Rayet, P. Descouvemont, D. Baye, C. Leclercq-Willain, A. Coc, S. Barhoumi, P. Aguer, C. Rolfs *et al.*, Nucl. Phys. **A656**, 3 (1999).

[3] M. S. Basunia, E. B. Norman, H. A. Shugart, A. R. Smith, M. J. Dolinski, and B. J. Quiter, Phys. Rev. C **71**, 035801 (2005).

[4] Zs. Fülöp, A. Z. Kiss, E. Somorjai, C. E. Rolfs, H. P. Trautvetter, T. Rauscher, and H. Oberhummer, Z. Phys. A **355**, 203 (1996).

[5] W. Rapp, M. Heil, D. Hentschel, F. Käppeler, R. Reifarth, H. J. Brede, H. Klein, and T. Rauscher, Phys. Rev. C **66**, 015803 (2002).

[6] Gy. Gyürky, G. G. Kiss, Z. Elekes, Zs. Fülöp, E. Somorjai, A. Palumbo, J. Görres, H. Y. Lee, W. Rapp, M. Wiescher, N. Özkan, R. T. Güray, G. Efe, and T. Rauscher, Phys. Rev. C **74**, 025805 (2006).

[7] N. Özkan, A. St. J. Murphy, R. N. Boyd, A. L. Cole, M. Famiano, R. T. Güray, M. Howard, L. Sahin, J. J. Zack, R. deHaan, J. Görres, M. C. Wiescher, M. S. Islam, and T. Rauscher, Nucl. Phys. **A710**, 469 (2002).

[8] N. Özkan, G. Efe, R. T. Güray, A. Palumbo, J. Görres, H. Y. Lee, L. O. Lamm, W. Rapp, E. Stech, M. Wiescher, Gy. Gyürky, Zs. Fülöp, and E. Somorjai, Phys. Rev. C **75**, 025801 (2007).

[9] S. Harissopulos, A. Lagoyannis, A. Spyrou, Ch. Zarkadas, G. Galanopoulos, G. Perdikakis, H.-W. Becker, C. Rolfs *et al.*, J. Phys. G: Nucl. Part. Phys. **31**, S1417 (2005).

[10] E. Somorjai, Zs. Fülöp, A. Z. Kiss, C. E. Rolfs, H. P. Trautvetter, U. Greife, M. Junker, S. Goriely, M. Arnould, M. Rayet, T. Rauscher, and H. Oberhummer, Astron. Astrophys. **333**, 1112 (1998).

[11] C. Arlandini, F. Käppeler, K. Wisshak, R. Gallino, M. Lugaro, M. Busso, and O. Straniero, Astrophys. J. **525**, 886 (1999).

[12] K. Wisshak, F. Voss, Ch. Theis, F. Käppeler, K. Guber, L. Kazakov, N. Kornilov, and G. Reffo, Phys. Rev. C **54**, 1451 (1996).

[13] N. Prantzos, M. Hashimoto, M. Rayet, and M. Arnould, Astron. Astrophys. **238**, 455 (1990).

[14] W. Howard, B. Meyer, and S. Woosley, Astrophys. J. **373**, L5 (1991).

[15] P. E. Koehler, J. A. Harvey, R. R. Winters, K. H. Guber, and R. R. Spencer, Phys. Rev. C **64**, 065802 (2001).

[16] O. Bersillon, SCAT2 optical model code, OECD-NEA-DB-CPS, package ID: NEA0829/03 (1991).

[17] P. G. Young, E. D. Arthur, and M. Chadwick, GNASH-FKK statistical model code, OECD-NEA-DB-CPS, package ID: PSR-0125/07 (1998).

[18] T. Rauscher and F. K. Thielemann, At. Data Nucl. Data Tables **79**, 47 (2001); URL: http://nucastro.org/nonsmoker.html.

[19] I. Cata-Danil, N. V. Zamfir, M. Ivascu, D. Bucurescu, Gh. Cata-Danil, T. Glodariu, G. Suliman, L. Stroe, D. Ghita, C. Mihai, and T. Sava, Rom. Rep. Phys. **59**, 377 (2007).

[20] I. Cata-Danil, M. Ivascu, T. Glodariu, N. V. Zamfir, D. Bucurescu, D. Filipescu, G. Cata-Danil, L. Stroe, C. Mihai, D. Ghita, G. Suliman, and T. Sava, Rom. Rep. Phys. **60**, 555 (2008).

[21] ENSDF (Evaluated Nuclear Structure Data File), http://www.nndc.bnl.gov/ensdf/

[22] A. J. Morton, S. G. Tims, A. F. Scott, V. Y. Hansper, C. I. W. Tingwell, and D. G. Sargood, Nucl. Phys. **A537**, 167 (1992).

[23] J. F. Ziegler, J. P. Biersack, and U. Littmark, *The Stopping and Range of Ions in Solids* (Pergamon, New York, 1985).

[24] O. Sima, D. Arnold, and C. Dovlete, J. Radioanal. Nucl. Chem. **248** (2), 359 (2001).

[25] M. Avrigeanu, W. von Oertzen, A. J. M. Plompen, and V. Avrigeanu, Nucl. Phys. **A723**, 104 (2003).

[26] L. McFadden and G. R. Satchler, Nucl. Phys. **84**, 177 (1966).

[27] J. R. Huizenga and G. Igo, Nucl. Phys. **29**, 462 (1962).

[28] A. J. Köning and J. P. Delaroche, Nucl. Phys. **A713**, 231 (2003).

[29] RIPL, Section: Levels, ZA: 52121, 52120, 51120, 50117, NDS-IAEA.

[30] A. Gilbert and A. G. W. Cameron, Can. J. Phys. **43**, 1446 (1965).

[31] J. Kopecky and M. Uhl, NEA/NSC/Doc (95) 1, RIPL Segment VI, recommended file.